Synthesis of Alginic Acid−Poly[2-(diethylamino)ethyl methacrylate] Monodispersed Nanoparticles by a Polymer−Monomer Pair Reaction System

Rui Guo,† Leyang Zhang,† Zhiping Jiang,† Yi Cao,† Yin Ding,† and Xiqun Jiang*,†,‡

Laboratory of Mesoscopic Chemistry and Department of Polymer Science & Engineering, College of Chemistry & Chemical Engineering, Nanjing University, Nanjing, 210093, People's Republic of China, and Jiangsu Provincial Laboratory for Nanotechnology, Nanjing University, Nanjing, 210093, People's Republic of China

Received September 21, 2006; Revised Manuscript Received December 30, 2006

In this paper, alginic acid-poly(2-(diethylamino)ethyl methacrylate) (ALG−PDEA) nanoparticles were successfully prepared in aqueous medium using a polymer−monomer pair reaction system consisting of the anionic alginic acid (ALG) and the cationic 2-(diethylamino)ethyl methacrylate (DEA), without any aid of surfactants or organic solvents. The ALG−PDEA nanoparticles were monodispersed and stable in aqueous solution. Nanoparticles with desired size could be obtained by varying the amount of initiator or changing the concentration of reactants in solution, which renders this system highly controllable. After the ALG moiety was gelled by Ca^{2+}, the stability of the nanoparticles in basic or high salt concentration solutions could be notably enhanced. A pH-sensitive anticancer agent, hydroxycamptothecin (HCPT), was encapsulated in ALG−PDEA nanoparticles, and preliminary in vitro release as well as cytotoxicity experiments were carried out. It is found that this system seems to be a very promising carrier for the loading and delivery of labile drugs, taking into account that the preparation procedure is simple, mild, and organic solvent- and surfactant-free. Moreover, the abundant functional groups on the particle surface, such as carboxyls and hydroxyls, allow subsequent chemical modification, which may further unleash the potential of such a system in either biomedical applications or in the construction of other functional mesoscopic architectures.

Introduction

Nanoparticles with controlled size, shape, and chemical functionality have been required for numerous applications,[1−3] such as delivery of cancer chemotherapeutics and genetic therapy drugs.[4−6] Unfortunately, although several different routes, for examples the self-assembly of block copolymers in selective solvent[7,8] and microemulsion polymerization,[9−11] have been developed to prepare nanoparticles successfully, these strategies require the use of organic solvents and surfactants as well as sonication or homogenization, which greatly limits their applications in health-related fields. Hence, interpolyelectrolyte complexes (IPECs), which are formed spontaneously in aqueous medium due to the electrostatic interaction of oppositely charged polyions, have attracted particular interest because of not only their environment-friendly characteristic but also their ability to mimic the self-organization process in biological systems.[12] A number of studies have been devoted to artificial polyelectrolyte-based colloidal systems.[13−18] However, it is difficult to obtain stable monodispersed nanoparticles with specific size and structure because the formation and properties of IPECs depend heavily on too many parameters, such as the proportion of opposite charges, charge density, concentration, molecular weight of polyions, and the physicochemical environment.[19,20]

Utilizing the characteristics of IPECs, our group recently introduced a simple and direct approach to synthesize biocompatible nanoparticles of uniform size and structure without any aid of surfactants or organic solvents.[21−23] We used a water-soluble polymer−monomer pair composed of a cationic biomacromolecule, chitosan (CS), and an anionic monomer, acrylic acid (AA), as a reaction system. With the polymerization of the monomers, the electrostatic interaction between biomacromolecule and monomer turns into a stronger interaction between two oppositely charged polyions. When polymerization reaches a certain degree, the hollow CS−poly(acrylic acid) (CS−PAA) nanospheres, with positively charged CS as the outer shell and CS−PAA interpolyelectrolyte complex as the inner shell, were formed. Since this process is gradual and in pseudo-equilibrium, stable and hollow CS−PAA nanospheres could be obtained in aqueous solution.

Differently, in this work, we chose an anionic biomacromolecule, alginic acid (ALG), and a cationic monomer, 2-(diethylamino)ethyl methacrylate (DEA), to construct the polymer−monomer pair reaction system and successfully synthesized monodispersed alginic acid−poly(DEA) (ALG−PDEA) nanoparticles in aqueous medium. ALG is a biocompatible linear binary copolymer of (1−4)-linked residues of β-D-mannuronic (M) and α-L-guluronic (G) acids (the pK_a values for them are 3.38 and 3.65, respectively),[24] and it has been widely investigated as a kind of important biomaterial in many fields such as cell immobilization, tissue engineering, and drug delivery.[25−28] Despite the fact that some advances have been made in the preparation of alginate-based micro- and submicron particles, the synthesis of alginate nanoparticles, in particular, monodispersed ones with a size less than 300 nm, remains as a considerable technological challenge.[29] DEA is a water-soluble basic monomer with a pK_a of around 7.0−7.3. Thus, poly(DEA)-

* To whom correspondence should be addressed. Fax: 86 25 83317761, E-mail: jiangx@nju.edu.cn.

† Laboratory of Mesoscopic Chemistry and Department of Polymer Science & Engineering, College of Chemistry & Chemical Engineering.

‡ Jiangsu Provincial Laboratory for Nanotechnology.

10.1021/bm060906i CCC: $37.00
Published on Web 02/10/2007

Scheme 1. Chemical Structures of Alginic Acid (ALG) and 2-(Diethylamino)ethyl Methacrylate (DEA)[a]

Alginic acid

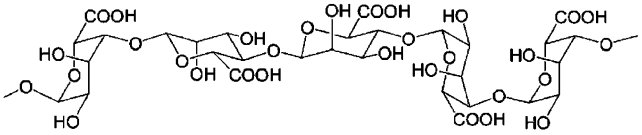

G M M G G

DEA

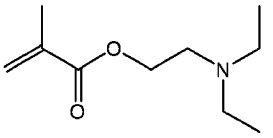

[a] M: β-D-mannuronic acid; G: α-L-guluronic acid. The molar fractions of guluronic acid residues (F_G), mannuronic acid (F_M), and sequence parameters given as the diad (F_{GG}, F_{MM}) were determined by NMR to be $F_G = 0.65$, $F_M = 0.35$, $F_{GG} = 0.53$, and $F_{MM} = 0.23$, respectively.[33]

based nanoparticles can exhibit a swelling−deswelling transition near physiological pH, making them valuable for biomedical applications.[30−32] Therefore, the obtained ALG−PDEA nanoparticles, by combining the advantages of both ALG and PDEA, may also have great potential in biomedical applications. Dynamic light scattering (DLS), transmission electron microscopy (TEM), and atomic force microscopy (AFM) were used to characterize these nanoparticles in aqueous medium and in the dry state. Factors that influence the formation and size of ALG−PDEA nanoparticles, including initiator amount, ratio, and concentration of ALG and DEA, were investigated in detail. In addition, Ca^{2+} was introduced as a biocompatible cross-linking agent to gel the ALG moieties at the outer shell so as to further improve the stability of ALG−PDEA nanoparticles. Taking into consideration the pH-sensitivity of both ALG and PDEA, changes in particle size were monitored in media at different pH values. Moreover, hydroxycamptothecin (HCPT), a potent anticancer drug, was encapsulated in the ALG−PDEA nanoparticles, and in vitro release and cytotoxicity tests of the drug-loaded nanoparticles were also conducted.

Experimental Section

Materials. Sodium alginate (Beijing Stock of China Medicine Company) with a viscous-average molecular weight of 170 kDa and a molar fraction of guluronic acid residues of 0.65 was refined twice by dissolving it in distilled water followed by precipitating with ethanol.[33] The precipitate was then dried in vacuum at 60 °C for 48 h and stored at 4 °C till use. ALG was obtained by acidification of sodium alginate with 0.1 M HCl before extraction with deionized water to remove residue ions. DEA (Adrich) was used as received. The chemical structures of ALG and DEA are shown in Scheme 1. Potassium peroxydisulfate ($K_2S_2O_8$) was recrystallized from deionized water before use. $CaCO_3$ was used as purchased from Shanghai Silian Chemical Company. Hydroxycamptothecin (HCPT) was a kind gift of Shanghai Institute of Materia Medica, Chinese Academy of Sciences, and used as received. All other reagents were of analytical grade and used without further purification.

Synthesis of ALG−PDEA Nanoparticles. A 2.5 g amount of ALG was first dissolved in 100 mL of DEA (2.7 g) solution in a three-neck flask under magnetic stirring. The ratio of ALG to DEA was kept at 1:1 ([carboxyl units]:[amino units]) except when otherwise stated. When the solution became homogeneous and clear, the temperature was raised to 70 °C under nitrogen flow, and a predetermined amount of $K_2S_2O_8$ solution (1%) was added to the system to initiate the polymerization of DEA monomers. We sampled the solution at different time intervals after the addition of $K_2S_2O_8$, and the sampled solution was immediately cooled with ice-bath. The bluish suspension was filtered with paper filter to remove any aggregations and dialyzed against 1 L of water (pH = 5.0) for 24 h using a dialysis bag with a cutoff molecular weight of 12 kDa to remove residual monomers before subsequent characterizations.

Physiochemical Characterizations. The pH measurements were performed with a Delta 320 pH-meter (Mettler Toledo Instruments Co., Ltd., Switzerland). Freeze-dried ALG−PDEA nanoparticles were obtained using a Labconco Freezone 6 freeze-drying system (Labconco). FT−IR spectra were collected on a Bruker IFS66V vacuum-type spectrometer to investigate the chemical interaction between ALG and PDEA. Samples were mixed with KBr powders and pressed to a plate for FT-IR measurement. The mean sizes of the nanoparticles were measured by the DLS method using a Brookhaven BI9000AT system (Brookhaven Instruments Corporation). All DLS measurements were done with a wavelength of 633.0 nm at 25 °C with a detection angle of 90°. Each sample was measured three times, and the results shown are the mean diameter for two replicate samples. The zeta potential of the nanoparticles was obtained with a Zetaplus (Brookhaven Instruments Corporation). The results were the average of three runs.

ALG−PDEA nanoparticles synthesized with different reaction time from 1 to 6 h were separated from the solution by centrifugation at 15000 rpm for 30 min. Then the sediments were dissolved by an aliquot of 0.2 M $Na_2CO_3/NaHCO_3$ buffer with a pH of 9.3. The resultant solutions were subject to molecular weight measurement by a gel permeation chromatography system (GPC) equipped with a static light scattering detector (DAWN HELEOS, Wyatt Technology Corporation) so that the absolute molecular weight of the PDEA could be obtained.

Morphological Studies. The morphologies of the samples were investigated by TEM (JEM-100S, JEOL, Japan) and AFM (SPI3800, Seiko Instruments Inc, Japan). For the TEM observation, properly diluted samples were placed onto a copper grid covered with a nitrocellulose membrane and air-dried. They were examined without any staining. In the AFM observation, one drop of properly diluted solution was placed on the surface of a clean silicon wafer and air-dried at room temperature. The images were obtained using a 20-μm scanner in tapping mode under ambient conditions. The phase images represent the variations of relative phase shifts and are thus able to distinguish materials by their intrinsic properties.

To study the interior structure of ALG−PDEA nanoparticles, microtomy was employed. A few granules of the freeze-dried sample were embedded in epoxy resin, and sections of about 70 nm thick were obtained by microtoming the resin sample at room temperature. Then the microtomed sections were subject to TEM observation.

Cross-Linking of Nanoparticles and Stability Assessment. To cross-link ALG−PDEA nanoparticles, the obtained suspension was dialyzed against saturated $CaCO_3$ aqueous solution for 4 h. The cross-linked product was dialyzed against distilled water for 72 h to remove the residual free Ca^{2+}. The stabilities of ALG−PDEA nanoparticles in media with different NaCl concentrations and pH values were assessed by dialyzing the nanoparticles against corresponding aqueous solutions for 48 h before particle size measurement and TEM observation.

Preparation and in Vitro Release of HCPT-Loaded ALG−PDEA Nanoparticles. The drug-loaded nanoparticles were prepared in a similar way as described above except that 2 mL of HCPT aqueous solution (0.5% w/v, pH = 8) were introduced into the ALG−DEA solution before polymerization. To investigate the effect of cross-linking on the release profile of drug-loaded nanoparticles, a certain amount of $CaCO_3$ was directly added into the reaction system after 1 h of polymerization, instead of dialysis against saturated $CaCO_3$ aqueous solution, so that unwanted drug release could be avoided during the dialysis process. The reaction was allowed to continue for another 1 h.

Unloaded drug and unreacted $CaCO_3$ solid were separated from the aqueous phase by filtration after reaction.

A Shimadzu LC-32010AD (Shimadzu) HPLC system equipped with a Lichrospher 321C-18, 5 μm, 200 mm × 4.6 mm RP-HPLC analytical 322 column was used to determine the HCPT concentration in solution. A Shimadzu RF 530 fluorescence detector, whose excitation and emission wavelengths were set at 385 nm and at 530 nm respectively, was adopted to enable the detection of HCPT at a rather low concentration (detection limit > 2 ng/mL) utilizing the drug's intense intrinsic fluorescence. The mobile phase was composed of 75/25 methanol (spectral grade, Merck, Germany)/double-distilled water (pH 5, adjusted with acetic acid), and the column was eluted at a flow rate of 1.0 mL/min at 35 °C. The concentrations of HCPT in all samples were determined according to the peak area at the retention time of 2.9 min by reference to a calibration curve.

In vitro release of HCPT from the nanoparticles was evaluated using a dialysis bag diffusion technique right after the preparation of drug-loaded nanoparticles. In order to avoid the dissolution saturation of HCPT in release medium, the nanoparticle solutions were first diluted to a concentration that corresponded to a HCPT concentration of about 20 μg/mL in release medium. Then 0.5 mL of the diluted solution was placed into a preswelled dialysis bag with a 12 kDa molecular weight cut off (Sigma) and immersed into 20 mL of 0.1 mol/L PBS (phosphate-buffered saline), pH 7.4, at 37 °C with gentle agitation. Thereby, the maximum HCPT concentration in the release medium was kept well below the saturation concentration (about 3 μg/mL at 37 °C in PBS, pH 7.4). Periodically, 1 mL of the release medium was withdrawn and then 1 mL of fresh PBS was added to the system. HCPT concentration in the sampled medium was determined by HPLC.

In Vitro Cytotoxicity of Empty Nanoparticles and HCPT-Loaded Nanoparticles in Comparison with Free HCPT. The in vitro cytotoxicity of empty nanoparticles, HCPT-loaded nanoparticles, and free HCPT were determined by standard MTT assays, and LoVo human colon cancer cell line was used. Cells were seeded in a 96-well plate at a density of 5000 cells per well and incubated at 37 °C in a humidified atmosphere with 5% CO_2. The culture medium was RPMI 1640 supplemented with 10% calf blood serum and was changed every other day until 80% confluence were reached. The medium was then replaced with 200 μL culture medium containing empty nanoparticles, HCPT-loaded nanoparticles and free HCPT at different concentrations. Empty nanoparticle concentration was set at the same value as the nanoparticle concentration used in the group of HCPT-loaded nanoparticle. One row of 96-well plates was used as control with 200 μL culture medium only. After incubation, 20 μL of 10 mg/mL 3-(4,5-dimethylthiazol-2-yl)-2,5-diphenyltetrazolium bromide (MTT) solution was added to each well, and the plate was incubated for 4 h, allowing the viable cells to reduce the yellow MTT into dark-blue formazan crystals, which were dissolved in 200 μL of dimethyl sulfoxide (DMSO). The absorbance of individual well was measured at 570 nm by an ELISA reader (Huadong, DG-5031, Nanjing). Cell viability was determined by the following formula:

$$\text{cell viability (\%)} = \frac{\text{Abs test cells}}{\text{Abs reference cells}} \times 100\%$$

where Abs is absorbance.

Results and Discussions

Preparation of ALG−PDEA Nanoparticles. In the present study, we prepared ALG−PDEA nanoparticles using a reaction system consisting of water-soluble ALG−DEA pairs. Alginic acid, instead of sodium alginate, was used in this study because the introduction of salt ions, such as Na^+ and Cl^-, would shield the charge of polymers and weaken the interaction between ALG and PDEA, hampering the formation of IPECs. This was confirmed by the fact that no nanoparticle was formed after the polymerization of DEA in sodium alginate solution. Although alginic acid is insoluble in water, DEA can help ALG to dissolve, because of its weak basic nature as well as the formation of polymer−monomer (ALG−DEA) pairs in solution. With the initiation by $K_2S_2O_8$, DEA was polymerized, and after polymerization for about 10 min, the solution changed from clear to bluish, indicating that ALG−PDEA nanoparticles appeared.

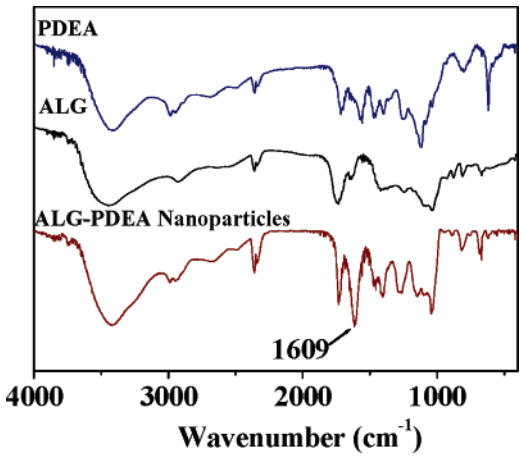

Figure 1. FT-IR spectra of PDEA, ALG, and ALG−PDEA nanoparticles.

According to our previous study,[33] the decomposition of $K_2S_2O_8$ causes a decrease in pH value of the solution, and as a result, alginate molecules in the solution assemble core−shell structural aggregates due to partial protonation of carboxyl groups. Actually, the pH value only went from 5.5 down to about 4.3 after 4 h of polymerization in the present case, owing to the buffer effect of the ALG−PDEA system, and this pH (4.3) was much higher than that required for alginate self-assembly. Thereby, the formation of nanoparticles during polymerization resulted purely from the electrostatic interaction between ALG and PDEA and had no relation to the minor drop of pH value. However, the slight decrease in the pH value of the solution during the polymerization can be exploited in the facile encapsulation of pH-sensitive anticancer agents in aqueous medium, as we will discuss later.

To investigate the interaction between ALG and PDEA, FT-IR studies were carried out. Figure 1 shows the FT-IR spectra of ALG, PDEA, and ALG−PDEA nanoparticles. The PDEA sample was synthesized by the same procedure as the preparation of ALG−PDEA nanoparticles except that ALG was omitted. In the IR spectrum of ALG−PDEA nanoparticles, the characteristic peak at 1609 cm^{-1} is assigned to the absorption band of carboxylate groups of ALG,[34,35] which form ionic bonds with the protonated diethylamino groups of PDEA. In contrast, this peak is much less pronounced in the spectrum of individual ALG and PDEA, indicating that a strong electrostatic interaction between the anionic ALG and the cationic PDEA does exist and ALG−PDEA nanoparticles are undoubtedly one kind of IPEC.

TEM and AFM observations were conducted to investigate the morphology and the structure of the ALG−PDEA nanoparticles, as shown in Figure 2. It is notable that all particles are well dispersed and in spherical shape with a uniform size of about 120 nm (Figure 2a), which is a little smaller than the data (165 nm) measured by DLS due to the dry state in TEM observation. The AFM topographic and phase images of ALG−PDEA nanoparticles are shown in Figure 2b and 2c, respectively. A spherical shape of ALG−PDEA nanoparticles is confirmed. Also, uniform radial hardness revealed in the phase image

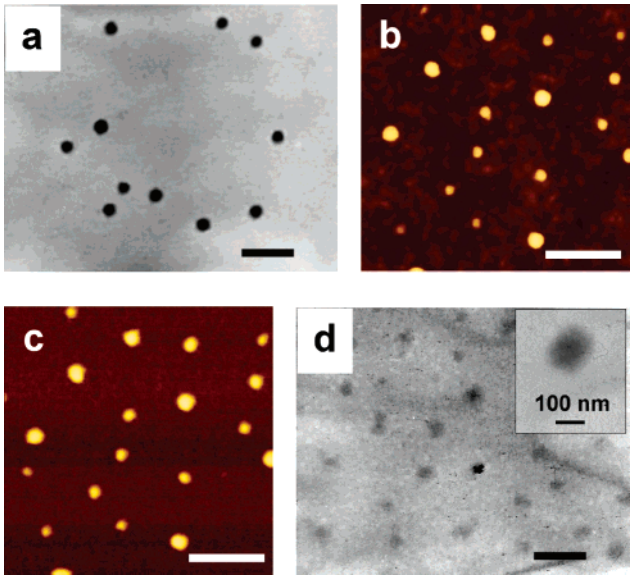

Figure 2. Morphologies of ALG−PDEA nanoparticles obtained after 120 min of polymerization. (a) TEM image; (b) AFM height image; (c) AFM phase image; (d) TEM image of microtomed section. Bars in a−d correspond to 500 nm. The inset in d is a micrograph of a single microtomed particle at a higher magnification.

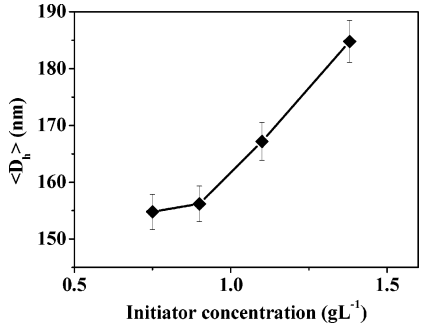

Figure 3. The average hydrodynamic diameter (D_h) of ALG−PDEA nanoparticles as a function of $K_2S_2O_8$ concentration in the reaction system.

(Figure 2c) indicates that the obtained nanoparticles have a solid structure. Figure 2d shows the TEM image of the microtomed section of ALG−PDEA nanoparticles. It is apparent that the nanoparticles obtained here are solid, which is in good accordance with the AFM phase image.

Control of Particle Size. Different amounts of $K_2S_2O_8$ were used to initiate the polymerization of DEA at 70 °C for 30 min to study the effect of initiator amount on particle size. The data detected by DLS are shown in Figure 3. When the $K_2S_2O_8$ concentration in the reaction system was lower than 0.5 g L^{-1}, no nanoparticle appeared. As the concentration increased from 0.75 to 1.4 g L^{-1}, the average hydrodynamic diameter of ALG−PDEA nanoparticles increases from 155 nm to about 185 nm. $K_2S_2O_8$ concentration higher than 1.4 gL^{-1} was not tested in order to eliminate the possibility of severe drop of medium pH caused by decomposition of $K_2S_2O_8$. The result obtained here suggests that particle size could be adjusted in a certain range by varying added initiator amount.

Since the ALG−PDEA nanoparticles are generated by the electrostatic interaction, the ratio of carboxyl units in ALG to amino units in DEA may be a key factor that influences particle properties. Table 1 shows mean diameters, scattering intensities, and zeta potentials of the nanoparticles synthesized with varied carboxyl:amino molar ratio from 1.5:1 to 1:1.5. The $K_2S_2O_8$ amount in each sample was fixed at a constant relative

Table 1. Mean Particle Size and Zeta Potential of ALG−PDEA Nanoparticles Obtained by Various Ratios of Carboxyl to Amino Group

carboxyl: amino	diameter ± SD (nm)	scattering intensity (kcps)[a]	polydispersity	zeta potential ± SD (mv)
1.5:1	105 ± 3	490.3	0.039	−57.5 ± 4.8
1:1	162 ± 3	1900.0	0.033	−56.1 ± 3.2
1:1.5	259 ± 3	289.2	0.061	−24.1 ± 3.6

[a] All samples were tested at the same concentration without any dilution.

Table 2. Mean Hydrodynamic Diameters of ALG−PDEA Nanoparticles Obtained with Different Concentrations of Reactants

ALG concn (gL^{-1})	diameter ± SD (nm)	scattering intensity (kcps)[a]	polydispersity
10.00	326 ± 5	570.6	0.078
7.50	275 ± 5	251.4	0.047
5.00	253 ± 4	148.1	0.068
2.50	161 ± 2	124.7	0.023
1.25	NA	NA	NA

[a] All samples were diluted 10 times before measuring.

concentration based on the content of DEA in solution. The highest ratio of carboxyl to amino was 1.5:1, above which alginic acid could not dissolve in water due to insufficient ionization. The average hydrodynamic diameters of ALG−PDEA nanoparticles increased markedly with increasing concentration of DEA in solution. However, the scattering intensity reached a maximum when the ratio was 1:1, meaning that the number of nanoparticles is the largest when the amount of cations in PDEA and that of anions in ALG are equal. In addition, at this ratio the resulting nanoparticles exhibited the best storage stability, and this further proves that the nanoparticles are formed by electrostatic interaction between ALG and PDEA. It should also be noted that the sample polydispersity index based on μ_2/Γ^2 is extremely low in each ratio of ALG to DEA, suggesting that the synthesized nanoparticles have a monodispersed characteristic. Meanwhile, the fact that zeta potentials of all the ALG−PDEA nanoparticles were highly negative not only explains the isolated state of nanoparticles seen in the TEM images but also provides some information about the microscopic structure of nanoparticles. The outermost layer of the nanoparticles should be the anionic ALG with ionized carboxyl groups that stabilize ALG−PDEA nanoparticles through electrostatic repulsion. When DEA was excessive, the zeta potential of nanoparticles was much lower, implying that the redundant DEA or PDEA may compromise the stability of nanoparticles by weakening the electrostatic repulsion. Therefore, the ratio of carboxyl to amino was set at 1:1 to obtain stable nanoparticles in the following experiments. Also noteworthy is that because of the IPEC nature of ALG−PDEA nanoparticles, the stirring rate during polymerization has a negligible effect on both particle size and polydispersity.

The concentrations of ALG and DEA in the reaction system also have a significant effect on nanoparticle size. Table 2 shows the summary of ALG−PDEA nanoparticles prepared with different concentrations of ALG and DEA after 60 min of polymerization. When the concentration of ALG was lower than 1.25 g L^{-1}, no nanoparticle was detected in solution by DLS. When the ALG concentration was in the range from 2.50 g L^{-1} to 10.00 g L^{-1}, the average hydrodynamic diameter of ALG−PDEA nanoparticles kept increasing from 161 to 326 nm, and the scattering intensity also increased correspondingly. Again, the polydispersity index was less than 0.1 for all samples, indicating that the prepared nanoparticles are monodispersed

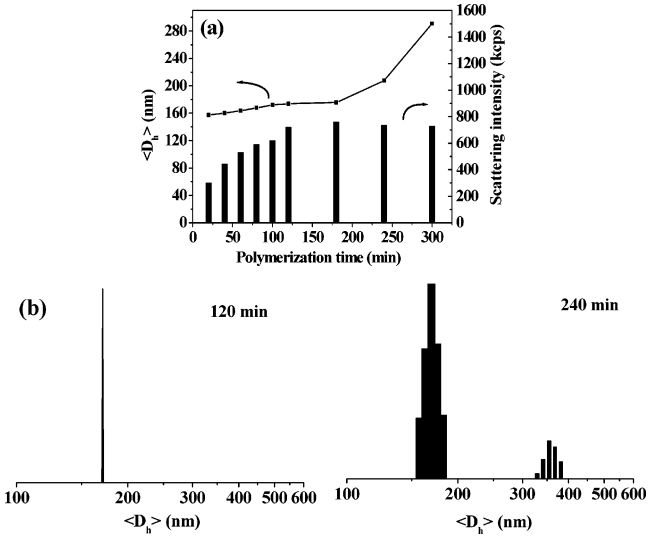

Figure 4. (a) The average hydrodynamic diameters and scattering intensities of ALG−PDEA nanoparticles as functions of polymerization time. (b) The hydrodynamic diameter distributions of nanoparticles formed at a polymerization time of 120 min and 240 min.

under different experimental conditions. Therefore, ALG−PDEA nanoparticles with the desired diameter and low polydispersity index can be obtained by simply varying the concentration of reactants.

The influence of reaction time on particle size was also investigated by DLS method. Figure 4a shows the average hydrodynamic diameters and scattering intensities of ALG−PDEA nanoparticles as a function of the reaction time. Before the initiation by $K_2S_2O_8$, no aggregate could be detected. After 10 min of polymerization, the solution changed from clear to slightly bluish, and the diameter of the assemblies was 157 nm at 30 min. The mean diameter slowly increased to only 172 nm after 180 min of polymerization, whereas the scattering intensity of the solution doubled. These indicate that in this period of time, nanoparticle size kept almost constant, but particle number increased dramatically with the polymerization of DEA. With further reaction, the particle size increased from 172 nm at 180 min to 290 nm at 300 min, while the scattering intensity began to decrease. The trend shown here can be explained by the fact that particles began to agglomerate with further extension of reaction time, whereas the increase in particle number had stopped. This is confirmed in Figure 4b, which shows the size distribution of nanoparticles at different polymerization times. In contrast to the monodispersed size distribution of nanoparticles at 120 min, nanoparticles at 240 min displayed a bimodal size distribution. One of the peaks occurs at 170 nm with a little broadening in the peak width, and the other one appears at 400 nm, which is attributed to the aggregation of nanoparticles. The TEM observation also corroborated that the increase of nanoparticle size was actually a result of interparticle coalescence (data not shown). Thus, reaction time has very limited effect on particle size, but too long a reaction time may result in unwanted particle aggregation. To keep the unimodal size distribution of nanoparticles and to minimize the aggregation between nanoparticles, a reaction time of 120 min is optimum.

Formation Mechanism of ALG−PDEA Nanoparticles. To get a deeper insight into the formation mechanism of ALG−PDEA nanoparticles, the molecular weight of PDEA in ALG−PDEA nanoparticles prepared with different reaction times was monitored, and the results are plotted in Figure 5. It can be found that the molecular weight of PDEA in ALG−PDEA

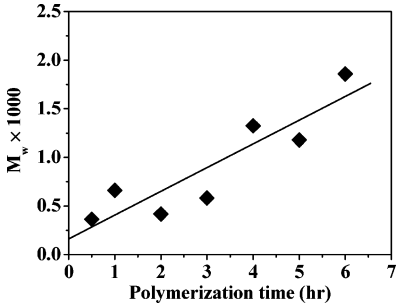

Figure 5. Dependence of molecular weight of PDEA in ALG−PDEA nanoparticles on polymerization time.

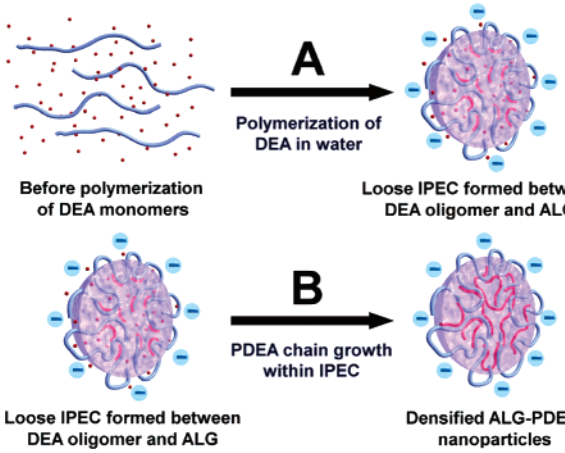

Figure 6. The formation mechanism of ALG−PDEA nanoparticle. Blue chains: ALG molecules; red dots: DEA monomers; red chains: PDEA molecules. The minus signs represent the negative charge on the particle surface imparted by ionized carboxyls in ALG molecules.

nanoparticles increases with polymerization time and is relatively low throughout the entire preparation.

Combined with the fact that the size of nanoparticles remained nearly constant in the first 3 h of polymerization while scattering intensity increased significantly as shown in Figure 4a, it is reasonable to propose a mechanism of ALG−PDEA nanoparticle formation as illustrated in Figure 6. Before polymerization, cationic DEA monomers are distributed around the chain of anionic ALG to help alginic acid dissolve, and polymer−monomer pairs are formed. Then, with the polymerization of DEA initiated by $K_2S_2O_8$, cationic PDEA appears. Once the molecular weight of PDEA reaches a certain critical value (about 300), the electrostatic interaction between the PDEA and ALG becomes strong enough to form a loose IPEC nanoparticle stabilized by an outer layer of ALG with ionized carboxyl groups. Hence, there are two locations for the DEA monomers to polymerize. (1) Initiation of the polymerization in the aqueous phase continues, and more oligomers of DEA are formed with polymerization. Therefore, more new IPEC nanoparticles are generated in the aqueous phase (process A in Figure 6), resulting in a fast increase of the particle number that is reflected by a rapid rise in scattering intensity in the beginning 2 h of polymerization (Figure 4a). Since IPEC is formed as soon as the molecular weight of PDEA reaches a certain critical value, all the newly formed IPEC nanoparticles would have a similar size, correlating well with the narrow size distribution reported by DLS measurements. (2) In the meantime, some DEA monomers that are inside those newly formed IPEC nanoparticles or diffuse into the loose IPECs from outside would participate in the polymerization within the particles (process B in Figure 6). Consequently, the molecular weight of PDEA

in nanoparticles increases with polymerization time, which would densify the nanoparticles. The growth of the molecular weight of PDEA would on the one hand increase the content within the particle, leading to a tendency of size expansion, and on the other hand, increase the electrostatic interaction forces between PDEA and ALG, resulting in another tendency of particle shrinkage. In our case, these two competing tendencies seem to be balanced well enough, and particle size remains nearly the same all through the polymerization.

It is also worth noting that, as opposed to the hollow structure observed in the CS−PAA system,[21−23] the ALG−PDEA nanoparticles obtained here are solid, as revealed in the TEM image of the microtomed section. This difference in structure might result from the difference in the magnitude of electrostatic interactions between the two nanoparticle systems. For the CS−AA system, before the polymerization of the AA monomer, the CS−AA micelles were formed and the particle size decreased during the polymerization of AA. Thus, the hollow structure could be explained by the equilibrium of two opposing forces, i.e., an electrostatic attractive force (between CS and PAA) to contract the spheres, and an electrostatic repulsive force from the charged shell to expand the spheres. However, in the present case, no ALG−DEA micelle was observed before the polymerization of the DEA monomer, and also the size of the ALG−PDEA particles did not decrease during the polymerization. Instead, the ALG−PDEA particles were formed only as the molecular weight of PDEA reached a certain critical value and the electrostatic interaction between the PDEA and ALG became strong enough. These differences imply that the electrostatic interaction between PDEA and ALG is weaker than that of the CS−PAA system. Accordingly, ALG−PDEA nanoparticles with a solid structure, but monodispersed in size, were formed.

Cross-Linking by Ca^{2+}. Although ALG−PDEA nanoparticles showed satisfactory storage stability and their size hardly changed even after 30 days in aqueous solution, these nanoparticles were found to be sensitive to ionic strength as well as pH value of the dispersing medium. They may be destroyed by the introduction of a large amount of ions or by an elevation of medium pH to above 8 as a result of the weakened interaction between ALG and PDEA. Therefore, proper cross-linking is mandatory to enhance the stability of ALG−PDEA nanoparticle. Since alginate makes a gel by the ionic bonding (called the 'egg-box structure') with divalent metal ions such as Ca^{2+}, and Ca^{2+}-alginate gel has many significant advantages in biological applications owing to its good biocompatibility,[36−38] herein Ca^{2+} is chosen to stabilize the nanoparticle by gelling ALG at the outer surface of nanoparticles. To avoid nanoparticle aggregation during Ca^{2+} addition, a saturated $CaCO_3$ solution was used in our study, considering that the concentration of Ca^{2+} in this solution is ten times lower than that of the carboxyl groups in ALG, as calculated from the solubility product constant (K_{sp}) of $CaCO_3$. Moreover, Ca^{2+} could be supplemented to the system continuously via dissolving solid $CaCO_3$ to compensate for the consumption of Ca^{2+} by gelling. Hence, the cross-linking could be proceeded in a very slow yet homogeneous manner to effectively avoid undesirable particle agglomeration.

Figure 7 shows the mean diameters of cross-linked and uncross-linked ALG−PDEA nanoparticles in solutions with different concentrations of NaCl. Both the cross-linked and uncross-linked nanoparticles got a little loosened with the introduction of NaCl. However, the cross-linked particles showed their advantage at higher ionic concentrations. When the concentration of NaCl was 0.3 mol L^{-1}, the mean diameter of uncross-linked nanoparticles was much larger than that of

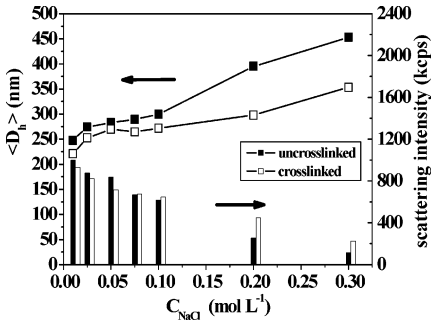

Figure 7. The mean diameter of cross-linked and uncross-linked ALG−PDEA nanoparticles as a function of NaCl concentration in aqueous solution.

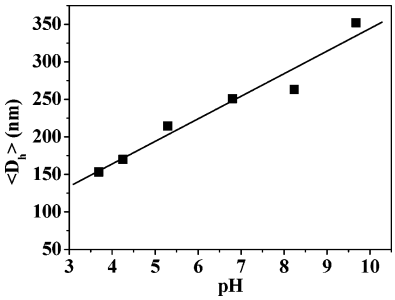

Figure 8. Influence of pH value of solution on the mean hydrodynamic diameter of cross-linked ALG−PDEA nanoparticles.

cross-linked ones, while the number of remaining nanoparticles was much less than the cross-linked counterparts, as deduced from the lower scattering intensity. Thus, using Ca^{2+} as a biocompatible cross-linker to gel the outer layer of ALG−PDEA nanaoparticles can improve their structural stability and their endurance against ions.

Since both ALG and PDEA are pH-sensitive, the pH value of the solution could affect the mean diameter of ALG−PDEA nanoparticles as shown in Figure 8. The cross-linked nanoparticles were used in this experiment for the reason that they are more stable in a broad range of pH compared to the uncross-linked ones which were completely destroyed when the medium pH was higher than 8. When the pH value of the solution was 3.83, the mean diameter of nanoparticles was 153.1 nm. With the increase of pH, the ALG moiety of the nanoparticles becomes more hydrated and extended due to deprotonation, whereas PDEA molecules would be gradually dehydrated and shrink. Therefore, the response of these nanoparticles to pH variation is a synergistic one contributed by both ALG and PDEA, and the particle size exhibits a pseudolinear dependence on medium pH, which is apparently different from the sudden size increase in the pH range of 4.5−8 observed in our previously reported alginate nanoparticle system.[33] When the medium pH went above 10, no particles could be detected. It seems that a covalent-bond-forming chemical cross-linking might be necessary if a higher stability is demanded.

In Vitro Release and Cytotoxicity of HCPT-Loaded ALG−PDEA Nanoparticles. HCPT is a topoisomerase I-targeted anticancer agent with poor water solubility. It can be hydrolyzed at neutral and basic pH into the water-soluble lactone-ring-opened carboxylate form, leading to a marked decrease in its antitumor activity and a significant increase in toxicity,[39] However, acidification of the carboxylate form of HCPT to a pH below 5 could reversibly convert the drug into its hydrophobic lactone form, as illustrated in Figure 9a.

Thus, by taking advantage of the aforementioned pH decrease accompanied by the polymerization due to the decomposition

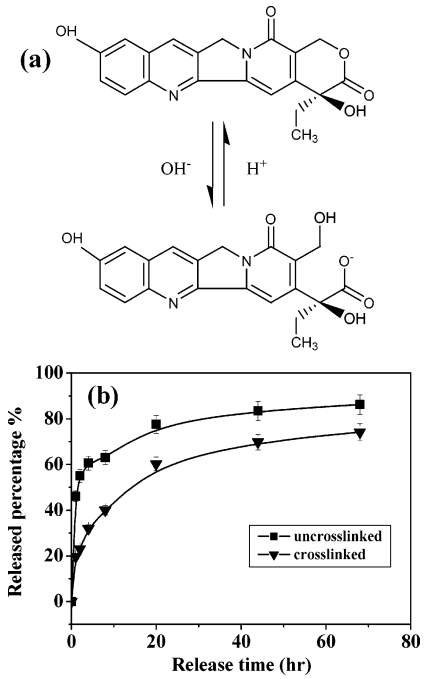

Figure 9. (a) The chemical structure of HCPT. (b) Release profiles of HCPT from uncross-linked and cross-linked ALG−PDEA nanoparticles at 37 °C, pH = 7.4.

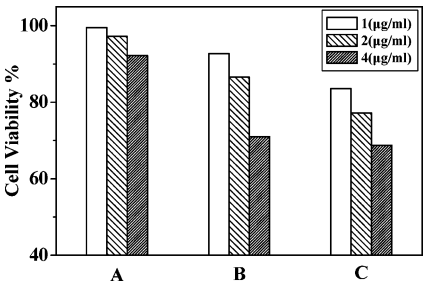

Figure 10. In vitro cytotoxicity of HCPT-loaded nanoparticles (B) in comparison with free HCPT (C) and empty nanoparticles (A). Empty nanoparticle concentration was set at the same value as the nanoparticle concentration used in the group of HCPT-loaded nanoparticles.

of $K_2S_2O_8$, we can start with the water-soluble carboxylate form of HCPT in neutral aqueous medium and then convert the drug into its water-insoluble lactone form gradually during reaction to achieve effective drug loading in the hydrophobic part of the ALG−PDEA nanoparticles. Drug loading efficiency of HCPT was 36%, and HPLC analysis revealed that the drug loading content was 2.7% (w/w). Figure 9b shows the release profile of HCPT from uncross-linked and cross-linked ALG−PDEA nanoparticles at 37 °C in PBS (0.1 M, pH 7.4). For the uncross-linked ones, an initial burst release followed by a slow release of HCPT was observed, and about 80% of the loaded HCPT was released from the ALG−PDEA nanoparticles within 24 h. This can be explained by nanoparticle swelling to a great extent, as mentioned earlier, in a medium containing a certain amount of ions at a pH value of 7.4. Hence, water exchange between the interiors of the swelled ALG−PDEA nanoparticles and the release medium is fast, leading to a fast drug release. In contrast, through proper cross-linking of the HCPT-loaded nanoparticles by Ca^{2+}, only about 60% of the loaded HCPT was released from nanoparticles within 24 h, and initial burst can be suppressed significantly.

To verify whether the released HCPT is still pharmacologically active, and to evaluate the cytotoxicity of the ALG−PDEA nanoparticles, in vitro cytotoxicity tests against LoVo cells were conducted. Cell viabilities of empty nanoparticles (A), HCPT-loaded nanoparticles (B), and free HCPT(C) at different concentrations are shown in Figure 10. Empty nanoparticle concentration was set at the same value as the nanoparticle concentration used in the group of HCPT-loaded nanoparticles. The result revealed that HCPT-loaded ALG−PDEA nanoparticles exhibited a similar cytotoxic activity of the free HCPT after a 24-h exposure time, whereas the empty nanoparticles were found to have no toxicity at the given concentration. Therefore, ALG−PDEA nanoparticles seem to be biocompatible and a very promising vehicle for the loading and delivery of labile drugs.

Conclusion

In this paper, ALG−PDEA nanoparticles were successfully prepared by polymerization of cationic DEA in the presence of anionic ALG, which represents a good generalization of our method of synthesizing nanoparticles by a reaction system consisting of water-soluble polymer−monomer pairs bearing opposite charges. The ALG−PDEA nanoparticles are uniform in size, well dispersed, and stable in aqueous solution. Nanoparticles with desired size can be obtained by varying the amount of initiator or changing the concentration of reactants in solution, which renders this system highly controllable. The stability of the nanoparticles against a basic environment and high salt concentration could be notably enhanced after the ALG shells were gelled by Ca^{2+}. Utilizing the pH decrease during the polymerization, HCPT was successfully encapsulated in ALG−PDEA nanoparticles, and preliminary in vitro release and cytotoxicity experiments were carried out. The results suggest that this system seems to be a very promising biocompatible vehicle for the loading and delivery of labile drugs (e.g., anticancer drugs and genes), taking into account that the preparation procedure is effective, simple, mild, and organic solvent- and surfactant-free. Moreover, the abundant functional groups on the particle surface, such as carboxyls and hydroxyls, allow subsequent chemical modification, which may further unleash the potential of such a system in either biomedical applications or in the construction of other functional mesoscopic architectures.

Acknowledgment. This work has been supported by the Natural Science Foundation of China (No.20374026, No. 50573031, 50625311, No.10334020) and the 973 Program of MOST (No.2003CB615600).

References and Notes

(1) Ulrich, R.; Du Chesne, A.; Templin, M.; Wiesner, U. *Adv. Mater.* **1999**, *11*, 141.
(2) Won, Y. Y.; Davis, H. T. L.; Bates, F. S. *Science* **1999**, *283*, 960.
(3) Allen, T. M.; Cullis, P. R. *Science* **2004**, *303*, 1818.
(4) Feng, S. S.; Chien, S. *Chem. Eng. Sci.* **2003**, *58*, 4087.
(5) Brigger, I.; Dubernet, C.; Couvreur, P. *Adv. Drug Delivery Rev.* **2002**, *54*, 631.
(6) Gref, R.; Minamitale, Y.; Peracchia, M. T.; Trubetskoy, V.; Torchilin, V.; Langer, R. *Science* **1994**, *263*, 1600.
(7) Cheng, K. W.; Chan, W. K. *Langmuir* **2005**, *21*, 5247.
(8) Hadjichristidis, N.; Iatrou, H.; Pitsikalis, M.; Pispas, S.; Avgeropoulos, A. *Prog. Polym. Sci.* **2005**, *30*, 725.
(9) Desgouilles, S.; Vauthier, C.; Bazile, D.; Vacus, J.; Grossiord, J. L.; Veillard, M.; Couvreur, P. *Langmuir* **2003**, *19*, 9504.
(10) Missirlis, D.; Tirelli, N.; Hubbell, J. A. *Langmuir* **2005**, *21*, 2605.
(11) Cade, D.; Ramus, E.; Rinaudo, M.; Auzely-Velty, R.; Delair, T.; Hamaide, T. *Biomacromolecules* **2004**, *5*, 922.

(12) Kabanov, V. A. Basic Properties of Soluble Interpolyelectrolyte Complexes Applied to Bioengineering and Cell Transformations. In *Macromolecular Complexes in Chemistry and Biology*; Dubin, P., Bock, J., Davies, R. M., Schulz, D. N., Thies, C., Eds.; Springer-Verlag: Berlin, Germany, 1994; p 151.
(13) Liu, X. H.; Yang, J. W.; Miller, A. D.; Nack, E. A., Lynn, D. M. *Macromolecules* **2005**, *38*, 7907.
(14) Izumrudov, V. A.; Wahlund, P. O.; Gustavsson, P. E.; Larsson, P. O.; Galaev, I. Y. *Langmuir* **2003**, *19*, 4733.
(15) Etrych, T.; Leclercq, L.; Boustta, M.; Vert, M. *Eur. J. Pharm. Sci.* **2005**, *25*, 281.
(16) Sergeyev, V. G.; Novoskoltseva, O. A.; Pyshkina, O. A.; Zinchenko, A. A.; Rogacheva, V. B.; Zezin, A. B.; Yoshikawa, K.; Kabanov, V. A. *J. Am. Chem. Soc.* **2002**, *124*, 11324.
(17) Izumrudov, V. A.; Zhiryakova, M. V. *Macromol. Chem. Phys.* **1999**, *200*, 2533.
(18) Oupicky, D.; Konak, C.; Ulbrich, K.; Wolfert, M. A.; Seymour, L. W. *J. Controlled Release* **2000**, *65*, 149.
(19) Tsuchida, E. *J. Macromol. Sci. Part A* **1994**, *31*, 1.
(20) Kotz, J.; Kopke, H.; Schmidt-Naake, G.; Vogl, O. *Polymer* **1996**, *37*, 2775.
(21) Hu, Y.; Jiang, X.; Ding, Y.; Chen, Q.; Yang, C. Z. *Adv. Mater.* **2004**, *16*, 933.
(22) Ding, Y.; Hu, Y.; Jiang, X.; Zhang, L.; Yang, C. *Angew. Chem., Int. Ed.* **2004**, *46*, 6369.
(23) Hu. Y.; Chen, Y.; Chen, Q.; Zhang, L.; Jiang, X.; Yang, C. *Polymer* **2005**, 46, 12703.
(24) Huguet, M. L.; Groboillot, A.; Neuffld, R. J.; Poncelet, D.; Dellacherie, E. *J. Appl. Polym. Sci.* **1994**, *51*, 1427.
(25) Orive, G.; Ponce, S.; Hernandez, R. M.; Gascon, A. R.; Igartua, M.; Pedraz, J. L. *Biomaterials* **2002**, *23*, 3825.
(26) Drury, J. L.; Mooney, D. J. *Biomaterials* **2003**, *24*, 4337.
(27) Lai, H.; AbuKhalil, A.; Craig Duncan, Q. M. *Int. J. Pharm.* **2003**, *251*, 175.
(28) Thu, B.; Bruheim, P.; Espevik, T.; Smidsrsd, O.; Soon-Shiong, P.; Skjåk-Bræk, G. *Biomaterials* **1996**, *17*, 1031.
(29) De, S.; Robinson, D. *J. Controlled Release* **2003**, *89*, 101.
(30) Amalvy, J. I.; Wanless, E. J.; Li, Y.; Michailidou, V.; Armes, S. P. *Langmuir* **2004**, *20*, 8992.
(31) Dai, S.; Ravi, P.; Tam, K. C.; Mao, B. W.; Gan, L. H. *Langmuir* **2003**, *19*, 5175.
(32) Wetering, P.; Cherng, J. Y.; Talsma, H.; Crommelin, D. J. A.; Hennink, W. E. *J. Controlled Release* **1998**, *53*, 145.
(33) Cao, Y.; Shen, X. C.; Chen, Y.; Guo, J.; Chen, Q.; Jiang, X. Q. *Biomacromolecule* **2005**, *6*, 2189.
(34) Moustafine, R. I.; Kemenova, V. A.; Van den Mooter, G. *Int. J. Pharm.* **2005**, *294*, 113.
(35) Sakugawa, K.; Ikeda, A.; Takemura, A.; Ono, H. *J. Appl. Polym. Sci.* **2004**, *93*, 1372.
(36) Dembczynski, R.; Jankowski, T. *Enzyme Microbiol. Technol.* **2002**, *31*, 111.
(37) Blandino, A.; Macias, M.; Cantero, D. *Process Biochem.* **1999**, *36*, 1081.
(38) Morre, M. L.; Maggi, L.; Vigo, D.; Galli, A.; Bornaghi, V., Maffeo, G.; Conte, U. *Biomaterials* **2000**, *21*, 1493.
(39) Garcia-Carbonero, R.; Supko, J. G. *Clin. Cancer Res.* **2002**, *8*, 641.

BM060906I